Combustion and Flame 197 (2018) 378–388

Contents lists available at ScienceDirect

Combustion and Flame

journal homepage: www.elsevier.com/locate/combustflame

Soot formation in diluted laminar ethene, propene and 1-butene diffusion flames at elevated pressures

Elizabeth A. Griffin, Ömer L. Gülder*

University of Toronto Institute for Aerospace Studies, 4925 Dufferin Street, Toronto, Ontario M3H 5T6, Canada

ARTICLE INFO

Article history:
Received 5 April 2018
Revised 4 June 2018
Accepted 18 August 2018

Keywords:
High-pressure soot
Sooting propensity of propene
Sooting propensity of 1-butene
Soot in olefin flame
High-pressure laminar flames

ABSTRACT

Soot formation characteristics of ethene, propene, and 1-butene, the most abundant unsaturated intermediates in thermal decomposition of paraffinic hydrocarbons, were investigated in laminar diffusion flames stabilized on a co-flow burner installed in a high-pressure combustion chamber with optical access. All three olefins were diluted with nitrogen to produce sooting but non-smoking diffusion flames at desired pressures. Pressure range was 1–2.5 bar with 1-butene, and 1–8 bar with propene and ethene. Upper pressure limits of 1-butene and propene were established by their respective vapour pressure characteristics. The spectral soot emission technique, in which radiation emitted by the soot within the flame was collected as line-of-sight intensity and spectrally resolved over the range 690–945 nm, was used to measure radially-resolved temperature and soot volume fraction. The carbon mass flow rates of the three fuels were kept constant at 0.505 mg/s to facilitate direct comparison among the fuels at elevated pressures. With the same dilution level, the sooting propensity increased from ethene to 1-butene as expected; however, the pressure sensitivity of propene and 1-butene differed significantly from that of ethene. Soot yields in both propene and 1-butene flames showed a much weaker dependence on pressure than the soot in ethene flames. In the decomposition of propene and 1-butene, allyl radical and 1,3-butadiene are known to form in critical quantities leading to formation of higher molecular growth species specifically six-membered ring aromatics, and presence of these simple aromatics is argued to play a role in lowering the pressure sensitivity of the soot in C_3 and C_4 olefin flames.

1. Introduction

The combustion engines used in air and ground transportation are designed to operate at pressures well above the atmospheric to benefit from higher thermal efficiencies and reduced space requirements in the vehicle. Formation of soot in engines operating mostly in non-premixed combustion mode is a current concern and soot emissions from the engine exhausts have negative implications for human health and climate change. In spite of the recent advances in our understanding of soot formation processes in combustion, we still do not possess a good handle of soot formation at elevated pressures. The situation is further complicated by the elusive kinetic processes involved in the high pressure combustion of transportation fuels such as diesel and jet fuel. To provide a better insight into the soot processes at elevated pressures, research involving tractable measurements of soot processes in laminar flames stabilized at high pressures seems to be one of the preferred approaches [1–7].

C_2–C_4 olefins, i.e., ethene, propene, and butene, are not among the common fuels used for practical combustion purposes, except for gasoline which may contain about 5–10% olefinic compounds; however, they are the most common olefins observed as intermediate species in the thermal decomposition and pyrolysis of larger molecule paraffinic hydrocarbons especially at temperatures above 1000 K, see e.g., [8–10]. Also, propene is one of the abundant hydrocarbons in industrial gas flares [11] which are commonly used for both emergency and routine destruction of combustible gases by open flame burning in petroleum refinery and chemical process industries, and formation and emissions of soot particles from such flares are a current environmental concern. As a result, there has been several recent studies of lower olefins in premixed and diffusion flames to gain further insight into their combustion chemistry, see e.g., [12–15].

Schalla et al. [16] and Schalla and McDonald [17] showed that sooting propensity of propene is second to that of butene which is the most prolific soot producer of the 1-olefins. At atmospheric conditions formation of soot precursors and soot processes show a strong dependence on fuel molecular structure [18–20]; however, it is not clear whether this fuel structure dependence characterized

* Corresponding author.
E-mail addresses: ogulder@utias.utoronto.ca, flame-utias7@usa.net (Ö.L. Gülder).

https://doi.org/10.1016/j.combustflame.2018.08.010
0010-2180/

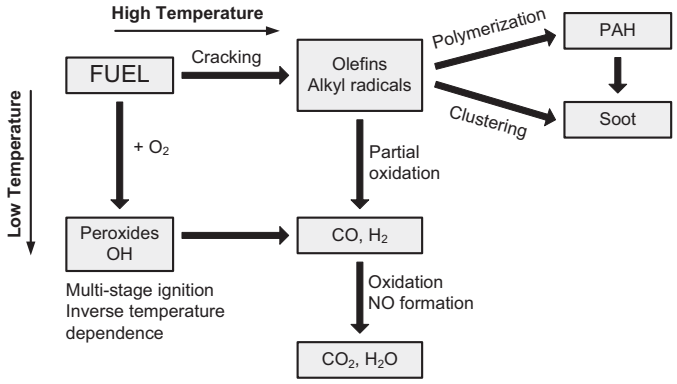

Fig. 1. Modelling approach to simulate cracking and auto-ignition in diesel engine combustion. The schematics is adopted from Yoshihara et al. [28].

at atmospheric conditions is carried into the high pressure combustion. If the pressure dependence of sooting propensity is not unique but fuel molecular structure specific, then this would have some implications for assessment of soot emissions from diesel and gas turbine engines.

The initiation step in the thermal cracking of paraffins seems understood well to be the homolytic scission of a C–C bond in the parent molecule producing two alkyl radicals [8–10,21,22]. The chain propagation involves hydrogen abstraction by the small free radical fragments from the reactant molecule to form the so called parent radicals and the subsequent decomposition of these radicals by scission of the C–C bond in beta position to the radical site. As a result, all but the simplest radicals decompose to yield an olefin and another alkyl radical. For example, in the thermal decomposition of *n*-hexadecane at 1033 K [21] and that of *n*-dodecane at 1050 K [9], it was found that C_2–C_4 alkenes were dominant intermediates in addition to hydrogen, methane, and ethane. As a result, the question of chemical kinetics of larger molecule paraffinic hydrocarbons can be handled at two stages for practical engineering applications. The first stage would involve the development of schemes for the purpose of estimating the products distribution of the thermal decomposition process as affected by the fuel chemical structure, pressure, and temperature. The schemes developed would make it possible to represent the fuel cracking rate with a relatively simple model as a function of fuel type, temperature and pressure involved in the process. The second stage will be the development of appropriate reaction models representing pyrolysis, oxidative pyrolysis, and oxidation of the products of initial fuel cracking at relevant pressures.

A similar situation exists in oxidation of paraffins, if the cracking reactions described above are fast enough [23]. As discussed by Minkoff and Tipper [24], in high-temperature combustion, many of the paraffinic molecules thermally decompose relatively fast before they start reacting directly with oxygen. Then the problem may be considered as the oxidation of lower carbon number olefins, in addition to hydrogen, methane, and ethane, after estimating the products distribution of the high-temperature fuel cracking, see e.g., [25–27]. This approach was applied to a diesel engine to model the fuel cracking and auto-ignition [28] and soot formation at high temperatures [29], as shown conceptually within the context of diesel engine combustion processes in Fig. 1. Calculated results agreed well with the measured induction periods in the high-temperature oxidation range [28] and with the measured soot profiles in shock tubes [29]. Recent studies decoupling the fuel pyrolysis from the oxidation of the decomposition products have resulted in promising outcomes [30–32]. Initial modelling efforts indicated that the approach provides a capability to estimate the extinction strain rates, ignition delays, and the laminar burning rates of aviation jet fuels [33].

Within the framework summarized in the previous paragraphs, the current work aims to provide insight into the soot formation processes in laminar diffusion flames of lower olefins at elevated pressures. Soot formation studies with propene and butene in diffusion flames are limited, and they are confined to atmospheric conditions. Detailed measurements of soot volume fraction and temperatures in co-flow laminar diffusion flames of ethene and propene, stabilized on burners manufactured from different materials were reported in [34]. In coflow laminar diffusion flames at atmospheric pressure fuelled by olefins (propene and ethene), soot volume fractions displayed a lower sensitivity to flame temperature than those in alkane flames (isooctane and propane) [35]. In a recent combined experimental and numerical study at atmospheric pressure, the soot and PAH formation tendencies of various 1-alkenes were reported for counterflow diffusion flames [15]. 1-butene was found to be the most sooting fuel of tested alkenes; the rest of them followed the ranking in decreasing sooting propensity as propene, 1-pentene, 1-hexene, 1-octene, and ethene [15], confirming the findings reported by Schalla et al. [16] and Schalla and McDonald [17]. Adding 1% by volume propene to a methane coflow diffusion flame at atmospheric pressure increased the maximum soot volume fraction by about 35% whereas the same amount of propane caused an increase about 17% [36]. In a counterflow diffusion geometry, adding propene to a base ethene flame showed increasing LII signals from soot as compared to the case of adding propane when the propene or propane mole fraction in base fuel ethene was kept under 4–5%, [12]. However, it was observed that upon addition of propane up to 50% to ethene increased PAH LIF signal more than propene addition; when the mole fraction of the added compound increased beyond 50%, then the PAH of propene added flames was higher than that of propane added flames [12].

The sensitivity to pressure of soot production in ethene diffusion flames have been studied previously [2,3,37–39] and it was demonstrated that the soot formation in ethene flames display a stronger dependence to pressure as compared to methane, ethane, and propane [37]. However, there has not been any study investigating the soot production in propene and butene diffusion flames at pressures above atmospheric. The experimental data on soot processes in tractable olefin flames at elevated pressures would be helpful in developing accurate kinetic mechanisms suitable for high pressure soot formation simulations.

In this work, sooting characteristics of lower olefins, i.e., ethene, propene, and 1-butene, in coflow laminar diffusion flames at elevated pressures are investigated experimentally. Olefins are diluted with nitrogen to have sooting but non-smoking flames at desired pressures. Soot yields and their variation with pressure are discussed and compared to the sooting characteristics of other hydrocarbons.

Current non-intrusive diagnostics capabilities do not permit spatially and temporaly resolved measurements of mixing rates in sooting atmospheric turbulent diffusion flames. Situation becomes more complex when the pressure is added as another variable. Pressure changes the turbulence characteristics of the flow field leading to changes in soot processes and altering the mixing rates. Studying laminar diffusion flames at high pressures, on the other hand, permits one to isolate the chemical effects of changing pressure from the physical influence of turbulence; however, this is only feasible if the experiments are designed to be tractable at pressures of interest. Then the information obtained from laminar flame studies at elevated pressures can be used in turbulent flames by invoking approximations like flamelet approach [40]. There has been several studies reported in the literature in recent years on soot formation at pressures above atmospheric in

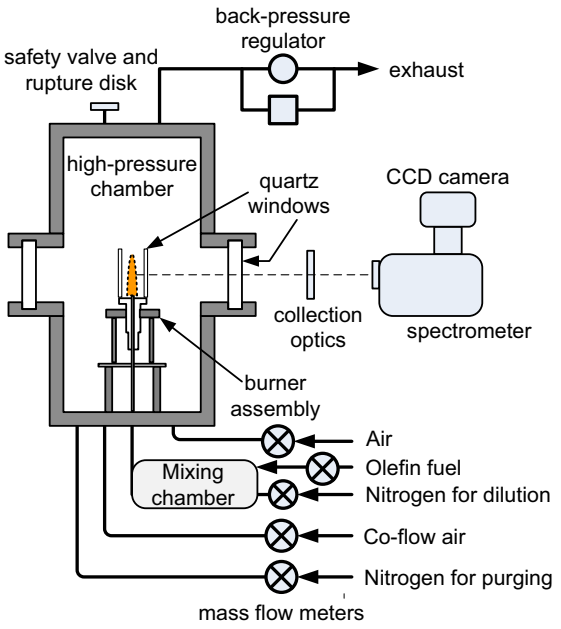

Fig. 2. A schematic diagram showing the main components of the high-pressure experimental rig.

tractable flames with various gaseous and liquid fuels, see e.g., [2,3,5,7,37,41–45] however, sensitivity of soot formation to pressure in propene and 1-butene flames are not available to the authors' knowledge.

2. Experimental methodology

A schematic diagram of the experimental rig is shown in Fig. 2. The flames of the three olefinic fuels were stabilized on a co-flow diffusion burner which has a fuel nozzle diameter of 3 mm surrounded by the co-flow air nozzle of 25 mm. Both fuel and air nozzles are fitted with porous metal inserts to provide top hat velocity profiles at the nozzle exits. The stainless steel burner rim is tapered to a fine edge to prevent the formation of any recirculation zones. The co-flow burner is mounted inside a high-pressure cylindrical combustion vessel with an internal diameter of 24 cm and a height of 60 cm. Optical access into the combustion chamber is provided by four circular ports, three of them fitted with quartz windows of 10 cm diameter, mounted on the side of the chamber making 90° angles between them, as shown in Fig. 2. The experimental rig was designed such a way that the diagnostics equipment is kept stationary and the combustion chamber is moved to map the whole flame. To move the combustion chamber to the desired measurement location, it is mounted on a three-dimensional translational stage which has a movement precision of 5 μm in each direction. Further details of the high-pressure combustion chamber and the co-flow diffusion burner are reported in the literature [39,42–48].

We used spectral soot emission technique, which is based on the two-colour flame pyrometry, to measure the radially-resolved temperatures and soot volume fractions [49]. For this purpose, line of sight soot emission intensities at wavelengths from 690 to 945 nm were recorded at 100 μm increments in the horizontal direction at a given height and at increments of 1 mm along the vertical flame axis. As shown in Fig. 2, blackbody radiation originating from the flame soot goes through a spectrometer and is registered on the CCD camera. The exposure time is based on the optimal intensity count registered on the CCD and for the current study it was about 1 s and the repeat images were recorded at each measurement location. These spectrally-resolved radiation intensities are binned with 21 nm widths and then inverted using an Abel type algorithm to obtain radially-resolved temperatures and soot volume fractions. Spectral soot emission technique and the Abel type inversion algorithm details can be found in our previous publications, see e.g., [41,43,49].

Table 1
Mass flow rates of co-flow air and the fuels. $\dot{m}_F$ = mass flow rate of the fuel; $\dot{m}_C$ = carbon mass flow rate; $\dot{m}_a$ = co-flow air mass flow rate.

Fuel	$\dot{m}_F$ (mg/s)	$\dot{m}_C$ (mg/s)	$\dot{m}_a$ (g/s)	Pressure (bar) at 1:2 dilution	Pressure (bar) at 1:3 dilution
Ethene	0.59	0.505	0.2	1–8	
Propene	0.59	0.505	0.2	1–4	4–8
1-Butene	0.59	0.505	0.2	1–2.5	

The gaseous olefins used as fuels in this study were research grade hydrocarbons. The mass flow rates of the fuels and the compressed air were metered by using mass flow controllers (Brooks SLA5850). These mass flow controllers were calibrated before each experimental run using a positive displacement calibration unit (Mesalabs Bios DryCal Definer 220) whose accuracy is traceable to NIST.

For all three olefins, the mass flow rates of the fuel feed to the burner were kept constant at 0.59 mg/s at all pressure conditions. The experimental conditions and the flow rates are listed in Table 1. The reason behind the constant mass flow rate of the fuel is that the soot measurements at different pressures are comparable to assess the influence of pressure if the flames are buoyancy-dominated [50]. In buoyancy-dominated laminar diffusion flames, the flame height and hence the residence time are not sensitive to pressure when the mass flow rate of the fuel is kept constant. The flame centerline velocities are similar along the flame's vertical axis at different pressures if the mass flow rate of the fuel is kept constant, see, e.g., [38,44].

It should be noted that the pressure ranges of each olefin and the nitrogen dilution ratios listed in Table 1 are dictated by thermophysical properties of the olefins and their sooting propensities. For example, the propene flame diluted with nitrogen at 1:2 mass ratio becomes a smoking flame above 4 bar pressure. Therefore, at 4–8 bar pressures, propene is diluted with nitrogen at 1:3 mass ratio. For 1-butene, it is not possible to go beyond 2.5 bar pressure, because of the vapour pressure of 1-butene, above which 1-butene is no longer in the vapour phase [51,52].

3. Results and discussion

3.1. Flame shapes and temperatures

Still pictures of the propene and 1-butene flames at various pressures are shown in Figs. 3, and 4. Flame pictures of ethene (at 1 to 8 bar) and propene (at 4–8 bar) are not shown. Pictures of laminar diffusion flames of ethene at elevated pressures are available in previous publications [37,44,53]. The flame diameter was found to decrease in size becoming thinner as the pressure was increased. It has been established that along the height above the burner rim flame diameter scales with the inverse of the square root of pressure [1,42]. The visible flame heights showed some variation from atmospheric to 8 bar, however the stoichiometric heights are expected to be invariant with pressure, see, e.g., [38,50], in view of the fact that the mass flow rates of the fuels were kept constant at all pressures. Flame pictures exhibit soot containing areas, noticeable by the yellow glow, expanding closer to the burner rim as the pressure is increased for all cases, Figs. 3 and 4.

Fig. 3. Still pictures of propene flames at a dilution ratio of 1:2 by mass nitrogen from 1 to 4 bar.

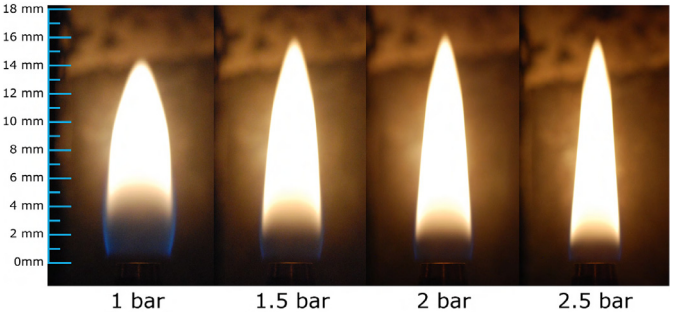

Fig. 4. Still pictures of butene flames at a dilution ratio of 1:2 by mass nitrogen at pressures from 1 to 2.5 bar.

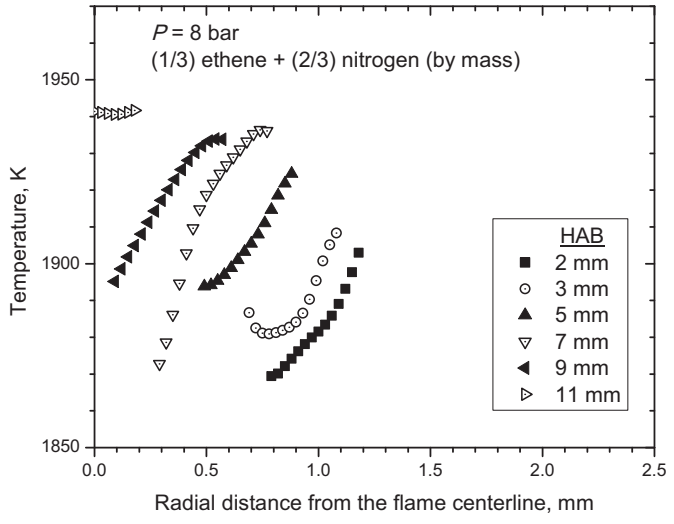

Fig. 5. Radial distributions of soot volume fraction at various heights above the burner exit at 8 bar in ethene flames.

A set of representative radial temperature profiles for the nitrogen-diluted ethene, propene, and 1-butene flames are shown in Figs. 5–7. Selected conditions for each olefin correspond to the pressures and heights above the burner exit for representative radial soot volume fraction figures that will be presented in Section 3.2. The maximum temperatures seems to stay around 1900 K in propene and 1-butene flames, Figs. 6 and 7 whereas it is well above 1900 K in ethene flames, Fig. 5. The relatively higher temperatures observed in ethene flames is a manifestation of the lower soot concentrations (that will shown in the next section) leading to relatively lower radiative heat losses from the flame.

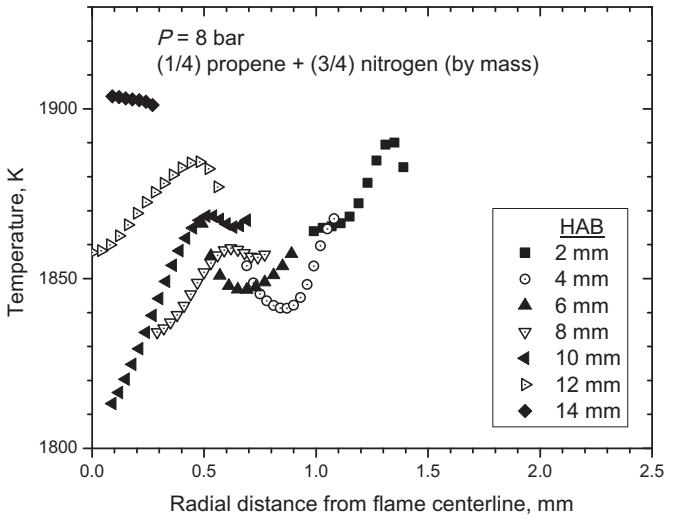

Fig. 6. Radial distributions of soot volume fraction at various heights above the burner exit at 8 bar in propene flames.

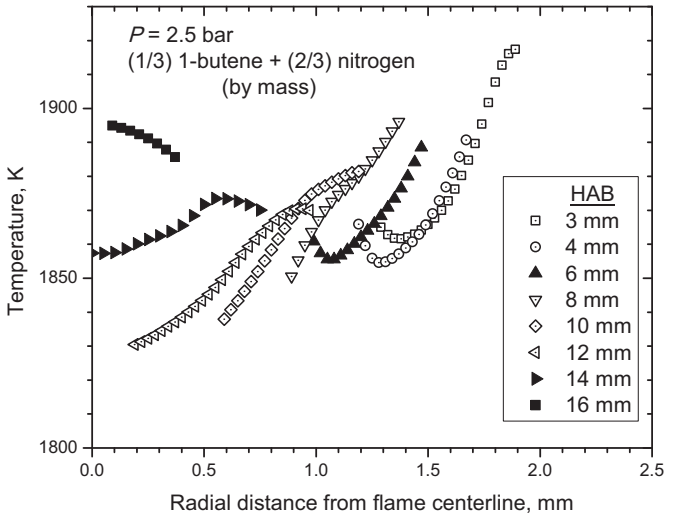

Fig. 7. Radial distributions of soot volume fraction at various heights above the burner exit at 2.5 bar in 1-butene flames.

The radial temperature profiles shown in these figures are similar to the profiles exhibited by diffusion flames at elevated pressures [41,42].

Although radially-resolved temperature profiles of the soot containing regions of the flame yield detailed thermal structure, a global flame temperature as a function of the height above the burner could provide a compact qualitative description of the thermal structure of the flame [54]. Traditionally, the line-of-sight integrated temperature was commonly used in analysis of the soot formation in laminar diffusion flames, see e.g., [55–58]. In axisymmetric laminar diffusion flames, line-of-sight integrated temperature along the flame height permits qualitative comparisons among flames fuelled by different hydrocarbons or among flames with different levels of inert dilution [59,60].

Line-of-sight integrated temperatures in propene flames along the height above the burner at various pressures display a structure similar to results reported previously [37,41], Fig. 8. It is apparent that line-of-sight temperature decreases with increasing pressure as a result of increasing soot radiation,

The temperature results for 1-butene flames are displayed in Fig. 9 for propene to nitrogen mass ratio of 1/2. The overall

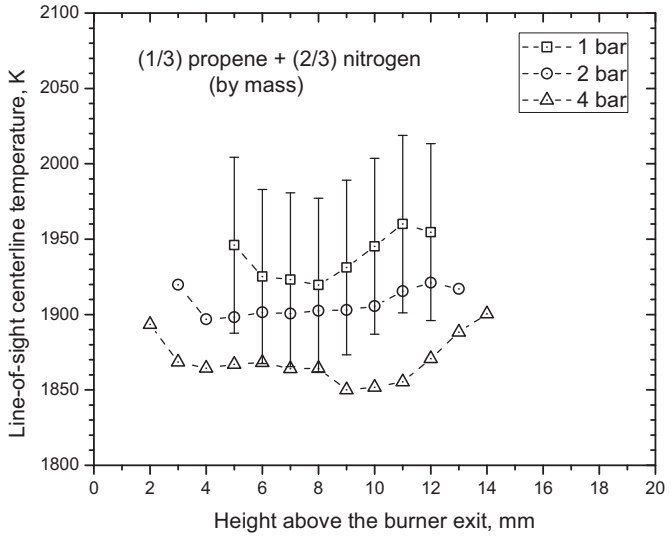

Fig. 8. Soot temperatures in propene flames at 1, 2, and 4 bar along the flame axis. Temperatures represent line-of-sight integrated values across the corresponding flame diameter.

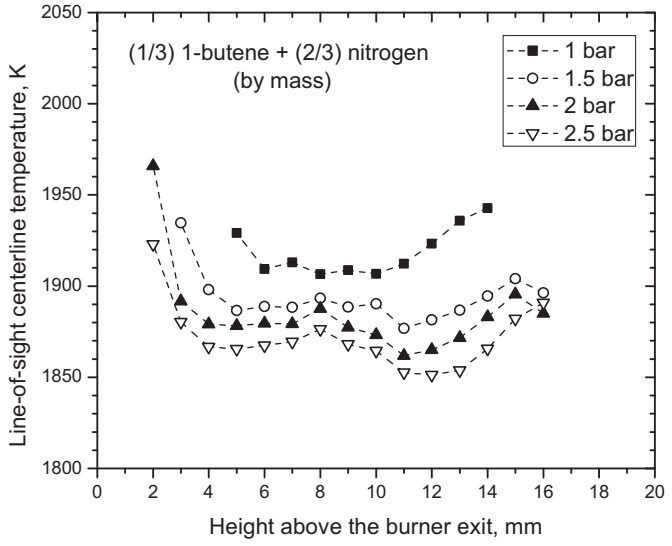

Fig. 9. Soot temperatures in 1-butene flames at 1, 1.5, 2, and 2.5 bar along the flame axis. Temperatures represent line-of-sight integrated values across the corresponding flame diameter.

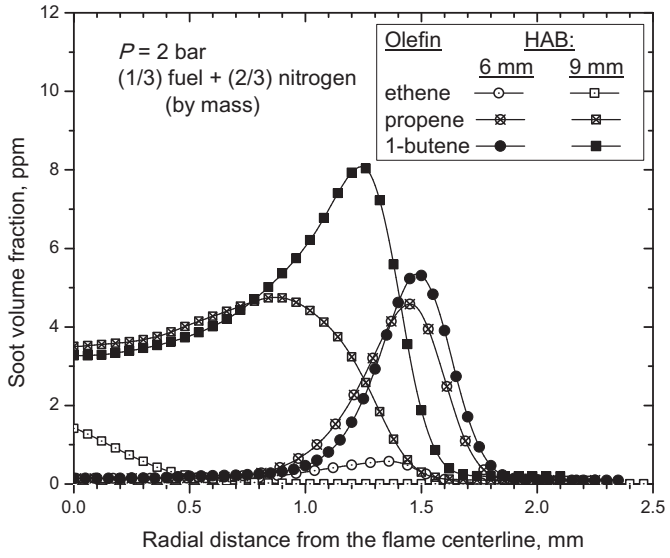

Fig. 10. Soot volume fraction profiles along the radial distance in ethene, propene, and 1-butene flames at 2 bar pressure. HAB represents the height above the burner exit along the flame centerline.

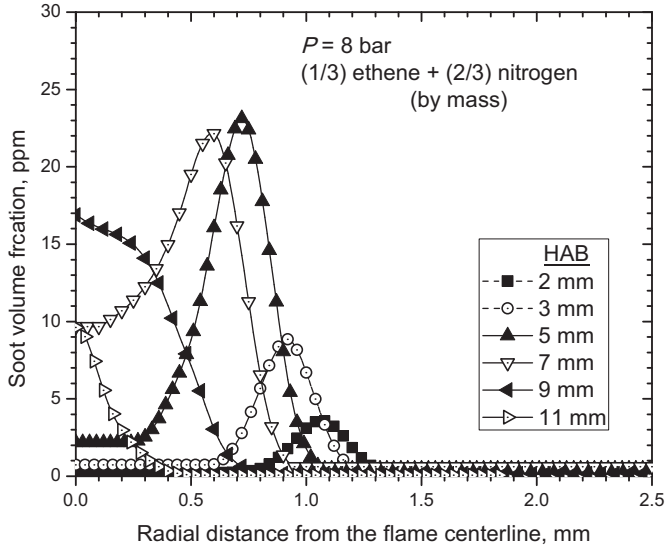

Fig. 11. Soot volume fraction profiles along the radial distance in ethene flame at 8 bar pressure. HAB represents the height above the burner exit along the flame centerline.

behaviour of the line-of-sight temperatures with height above the burner and pressure is qualitatively similar to those of propene.

Soot formation processes in diffusion flames are strongly influenced by temperature [35]. The influence of pressure on flame temperature in the absence of soot is negligible for practical purposes. The increase in soot concentration with increasing pressure leads to enhanced radiation heat loss from the flame reducing its overall temperature. For example, in ethene flames from 1 bar to 8 bar, the line-of-sight flame temperature is suppressed by about 100 K at mid-height of the flames (not shown). This drop in temperature would counteract the soot enhancing effect of pressure to a certain extent; as a result, pressure dependency of soot processes would be underestimated. Since the temperature drops in all three olefins with increasing pressure are comparable for similar pressure drops, Figs. 8 and 9, it can be assumed that the pressure dependence underestimation would be similar in magnitude by a scale factor in all three fuel cases.

3.2. Soot volume fractions

Radially-resolved soot volume fraction distributions, obtained from the spectral soot emission data, at various heights above the burner exit display a structure typical of laminar diffusion flames. For a quick comparison of the sooting propensities of the three olefins, radially-resolved soot volume fractions at 2 bar pressure are shown in Fig. 10 at heights of 6 and 9 mm above the burner exit. The higher soot production capacity of 1-butene in comparison to propene and ethene is apparent in Fig. 10, not only at the two heights shown here, but at all other heights at which measurements were taken (not shown in the figure). Soot volume fraction profiles along the radial distance from the flame centerline in the ethene flame at 8 bar pressure are shown in Fig. 11 at various heights above the burner exit. The radial distribution of soot volume fraction is annular in structure centered around $r = 1$ mm, where r is the radial distance from the flame axis, at heights of 2

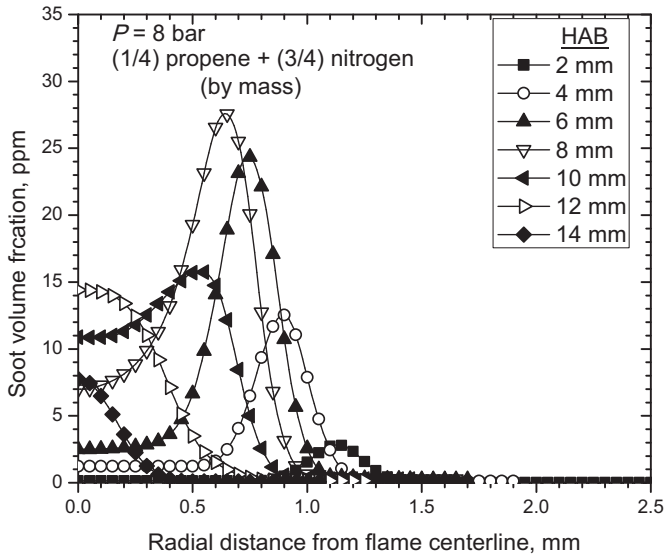

Fig. 12. Soot volume fraction profiles along the radial distance in propene flame at 8 bar pressure. HAB represents the height above the burner exit along the flame centerline.

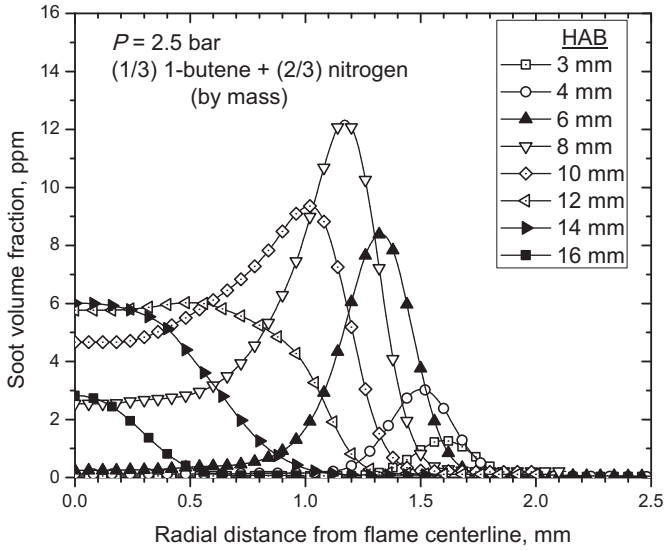

Fig. 13. Soot volume fraction profiles along the radial distance in 1-butene flame at 2.5 bar pressure. HAB represents the height above the burner exit along the flame centerline.

and 3 mm. There is negligible soot in the core of the flame. With increasing height, starting at about 5 mm, the peak of the annular soot volume fraction distribution shifts gradually towards the flame centerline as the peak soot volume fraction increases. Additionally, soot is measured closer to the flame centerline; at about $z = 5$ mm, where z is the height above the burner exit, soot is detected at the flame centerline. With further increase in height, the soot volume fraction in the core region of the flame grows while the soot concentration in the annular region drops. At $z = 9$ mm and above, the annular structure in the soot volume fraction distribution disappears and the highest soot volume fraction occurs on the burner centerline. The peak soot volume fraction in ethene flame observed at 8 bar pressure is about 26 ppm at $z = 8$ mm (not shown in Fig. 11).

The structure of the radially-resolved soot volume fraction distributions at various heights above the burner exit in propene flame at 8 bar is similar to that of ethene flame, Fig. 12. Note that the ratio of nitrogen to propene by mass is 3 in Fig. 12 whereas the ratio is 2 in the ethene flame. The maximum soot volume fraction in the propene flame occurs at $z = 8$ mm and is about 28 ppm.

As explained in the experimental method section above, the highest pressure that a 1-butene flame could be established at was 2.5 bar due to vapour pressure of 1-butene. The radial distributions of the soot volume fraction of 1-butene display the typical structure observed in ethene and propene flames and the maximum soot volume fraction is about 12 ppm at a height of 8 mm above the burner exit (Fig. 13).

The variations of the maximum soot volume fractions in the flames of ethene, propene, and 1-butene with pressure are depicted in Fig. 14. It is apparent that pressure dependence of maximum soot volume fraction is stronger in ethene flames in comparison to propene and 1-butene flames. However, it should be emphasized that when assessing the influence of pressure on soot processes, soot yield and its maximum value seem to be the proper metrics and they have been used in soot investigations carried out in high pressure flames and shock tubes. The next subsection of the paper addresses the rationale for this and describes the methodology of inferring soot yields before assessing the pressure dependencies of sooting in ethene, propene, and 1-butene flames.

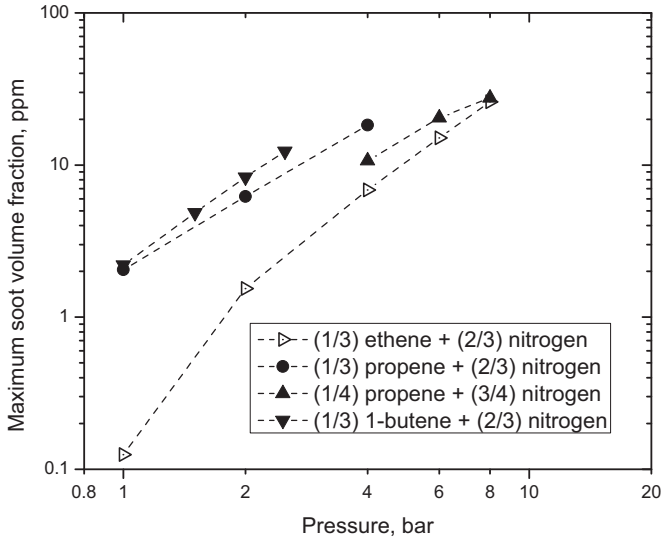

Fig. 14. Comparison of the maximum soot volume fraction of the ethene, propene, and 1-butene flames at various pressures on a logarithmic plot. Nitrogen dilution ratios are indicated in the legend.

3.3. Soot yields

Maximum soot volume fraction represents the local maximum anywhere in the flame envelope in units expressed as volume of soot per unit volume of gas. The soot yield, on the other hand, is obtained by integrating soot volume fraction across the flame radius and converting it to a mass fraction normalized by the carbon mass of the fuel stream. As a consequence, two flames with identical maximum soot volume fractions could have very different maximum soot yields if the radial soot volume fraction distributions are not the same. Most importantly, soot volume fraction would automatically scale with pressure even if there were no other effects of pressure on soot other than the volume change of the unit gas because of the fact that soot is incompressible for practical purposes. In contrast, the soot yield, and its maximum, would reflect chemical kinetic effects of pressure only on soot.

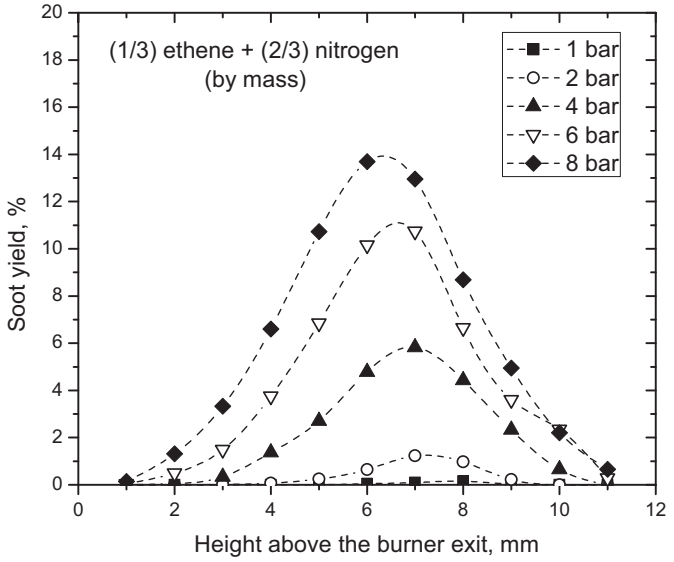

Fig. 15. Soot yield profiles of ethene flames at various pressures as a function of the height above the burner exit.

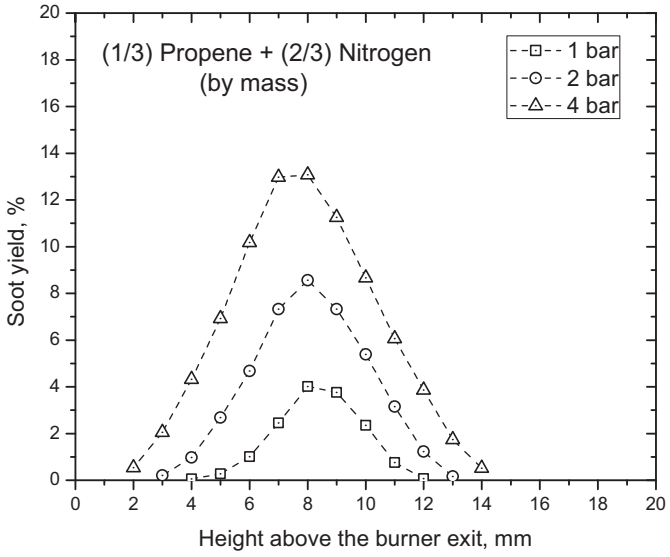

Fig. 16. Soot yield profiles of propene flames at 1, 2, and 4 bar as a function of the height above the burner exit.

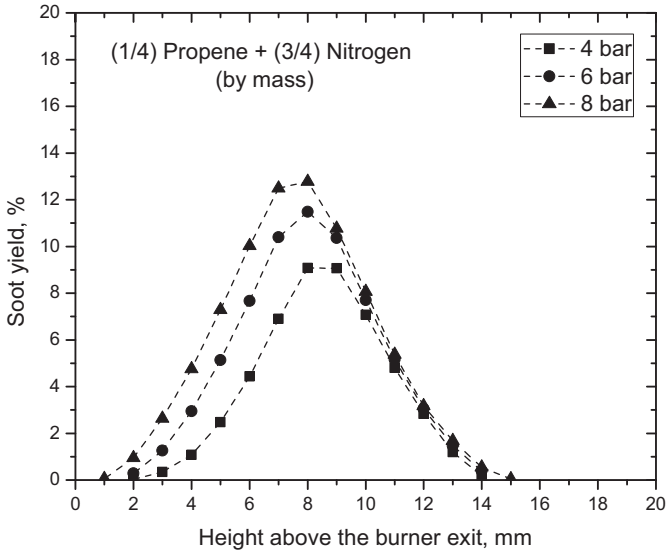

Fig. 17. Soot yield profiles of propene flames at 4, 6, and 8 bar as a function of the height above the burner exit.

The mass flux of soot, $\dot{m}_s$, at any height above the burner rim through the corresponding radial flame cross-section can be expressed as follows, if the radial soot volume fraction distribution and the velocity field at the cross-section of interest are known:

$$\dot{m}_s(z) = \rho_s \int 2\pi r f_v(r,z) v(r,z) \mathrm{d}r \tag{1}$$

The average density of soot, ρ_s, is taken as 1.8 g/cm^3 so that the current results are consistent with our previous studies [41,46]; f_v is the soot volume fraction; v represents the velocity field with radial and axial coordinates represented by r and z, respectively. Although the measurement of flow field within the envelope of laminar diffusion flames at pressures above atmospheric is a challenge, velocity data from detailed numerical simulations are available. It has been shown that the velocity field can be estimated by $(2az)^{1/2}$, where a is the acceleration induced by buoyancy. Using the velocity data from numerical simulations, we took $a \approx$ 41 m/s^2 in the current work, which is consistent with our previous publications, and further details are reported in references [61,62]. At a given fuel mass feed through the burner nozzle, the carbon mass flow, $\dot{m}_c$, at the burner exit will depend on the fuel's carbon content. Then, the soot yield at any height above the co-flow burner exit, Y_s, will be given by:

$$Y_s = \dot{m}_s(z)/\dot{m}_c \tag{2}$$

Soot yields can be evaluated from the radial soot volume fraction distributions and the approximate value of the acceleration constant discussed above using Eqs. (1) and (2).

The soot yield profiles shown in Fig. 15 along the height above the burner at various pressures in ethene flames display the strong influence of pressure on soot production. Peak soot yield shifts gradually from a height of 8 mm at 1 bar to 6 mm at 8 bar. Soot yields in propene flames in the pressure ranges of 1–4 bar and 4–8 bar are plotted in Figs. 16 and 17, respectively, at the dilution levels shown in the graphs. A weaker pressure dependence, especially between 4 and 8 bar, in comparison to soot yields in ethene flames is apparent. Soot yields in 1-butene flames, from 1 to 2.5 bar at 0.5 bar intervals, are displayed in Fig. 18. A qualitative comparison of soot yields of 1-butene to those of ethene implies a weaker pressure dependence of soot production in 1-butene flames.

To facilitate a direct comparison, the maximum soot yields of ethene, propene, and 1-butene are plotted in Fig. 19 on logarithmic scales to assess the pressure dependence of soot in olefinic diffusion flames. Also included in Fig. 19 are the maximum soot yield data for undiluted ethene from a previous study [37]. The pressure sensitivity of soot in diluted and undiluted ethene flames is almost identical, Fig. 19. However, in both propene and 1-butene flames pressure dependence is much weaker as compared to ethene flames. To provide an aid to guide the eye, reference slopes are included in Fig. 19. For ethene flames, between 1 and 3 bars the maximum soot yield scales as $P^{2.6}$ and as the pressure goes up the dependence gets weaker; between 4 and 8 bar it is $\approx P^{1.3}$. For propene and 1-butene, scaling is $\approx P^{1.1}$ from 1 to 2 bar, with increasing pressure dependence becomes weaker approaching to $P^{0.4}$ for pressures larger than 4 bar, Fig. 19. A significant decrease in pressure exponents from ethene to propene/1-butene is apparent and the probable reasons behind this finding will be discussed next.

One of the noticeable differences between ethene and propene/1-butene pyrolysis product compositions is that the

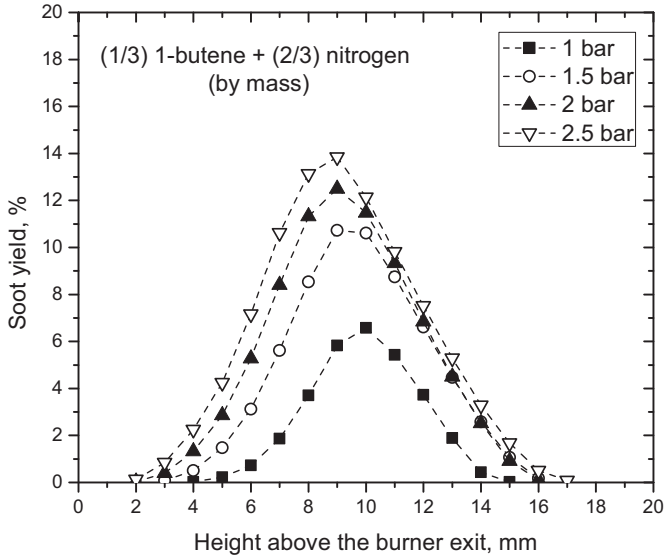

Fig. 18. Soot yield profiles of 1-butene flames at 1, 1.5, 2, and 2.5 bar as a function of the height above the burner exit.

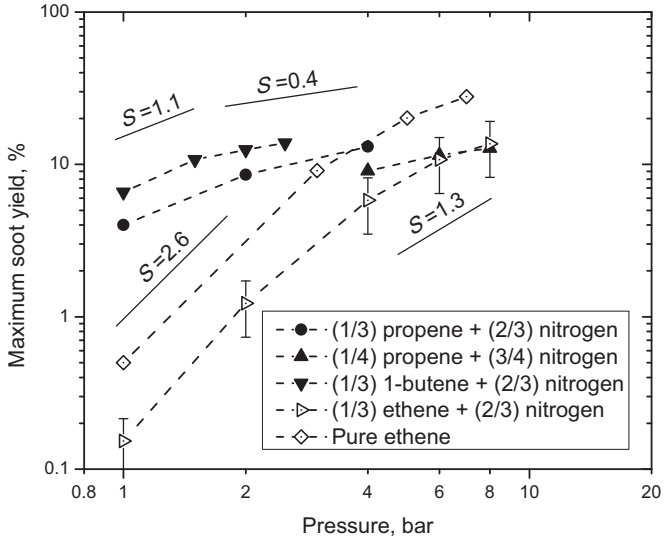

Fig. 19. Maximum soot yields of ethene, propene, and 1-butene flames at various pressures. Also included in the plot are the pure ethene data from Ref. [37]. Dilution ratios by mass are indicated in the legend. Reference lines (solid) with their respective slopes, *S*, are also shown on the graph to aid guiding the eye.

latter has a much higher amount of single ring aromatics and PAH [15,63,64]. A recent comprehensive combined experimental and numerical study to assess the sooting propensity of 1-alkenes in counterflow diffusion flames at atmospheric conditions concluded that the PAH measured by LIF at 400 nm followed the ranking 1-butene > propene > ethene [15], pointing to the higher levels of aromatics formation in propene and 1-butene diffusion flames as compared to ethene flames.

In the pyrolysis of propene, allyl radical, mainly formed through H-atom abstraction from the parent fuel by methyl and H atoms, plays a central role for product formation [63] and eventually leads to the formation of 1,3-butadiene. Similar to butane pyrolysis, 1,3-butadiene leads to formation of stable aromatic species. In the pyrolysis of butene, decomposition products contain a considerable quantity of 1,3-butadiene [64]. The importance of this is that a radical addition to the terminal carbon atom in the 1,3-butadiene molecule leads to formation of an adduct which is resonantly stabilized. Resonantly stabilized radicals, due to lowered energy required, play a crucial role in formation and growth of stable six-membered ring species, as discussed in detail by Wang et al. [64] and Sinha et al. [65].

It should be noted here that in low pressure (40 mbar) rich premixed flames of butene isomers oxidation pathways were shown to proceed through C_3 chemistry as well as C_4 [66]. It was emphasized that most of the benzene is formed through C_3 pathway in rich premixed 1-butene flame [66], in contrast to the dominant C_4 pathway found for benzene buildup in pyrolysis of 1-butene [64]. In another 1-butene pyrolysis study conducted at 9–16 mbar pressure [67], it is concluded that 1-butene is decomposed mainly through two reaction sequences 1-C_4H_8 → aC_3H_5 → aC_3H_4 → pC_3H_4 → C_2H_2 and 1-C_4H_8 → $saxC_4H_7$ → 1,3-C_4H_6 → C_2H_3 → C_2H_2, in which the former plays a more significant role. Although the dominant routes of decomposition and of benzene buildup in 1-butene pyrolysis have not been established yet firmly, there seems to be a consensus in formation of a significant amount of benzene [64,66,67].

In view of the nature of pyrolysis product compositions of propene and 1-butene discussed above, it would be instructive to look at the pressure sensitivities of soot production in aromatic hydrocarbons. In experiments that involved doping methane diffusion flames with toluene at various pressures, it was shown that the pressure dependence of soot becomes relatively weaker with toluene addition to the base fuel in comparison to *n*-heptane addition [68]. Although soot formation studies with aromatic hydrocarbons in high-pressure flames are scarce, there are pyrolysis and very rich premixed mixture studies with aromatic hydrocarbons in shock tubes. Soot measurements in toluene-argon mixtures behind reflected shock waves in the pressure range of 0.3–3 bar over the temperature range of from 1500 to 2300 K showed a measurable pressure effect [69]. However, in a similar shock tube study of toluene pyrolysis, but over the pressure range of 2.5–10 bar, a much weaker pressure effect on soot yield was observed [70,71]. These two sets of studies imply that pressure sensitivity of soot yield of toluene pyrolysis is present at lower pressures, up to 2–3 bar, however, between 2.5 and 10 bar little quantitative effect of pressure was found [71]. In shock tube studies of benzene pyrolysis, soot yield did not change significantly with pressure between 6 and 60 bar [72,73] similar to toluene pyrolysis experiments [71].

Therefore, there is strong evidence that pressure dependence of soot formation of single ring aromatic molecules is much weaker than that of alkanes. Since, propene and 1-butene pyrolysis produces larger amounts of aromatic species than ethene pyrolysis, lower sensitivity to pressure of aromatics could be the reason behind the bahaviour observed in Fig. 19.

Another noticeable difference reported between the pyrolysis products/intermediates of ethene and propene/1-butene is the acetylene concentrations; acetylene in the ethene products was found to be in larger quantities than those in propene/1-butene decomposition intermediates [15]. Guo et al. [4] described the role of acetylene in soot formation and argued that the rate of increase of acetylene is relatively slower as well as the formation rate of H atom with increasing pressure in ethene diffusion flames. This manifests itself as a slower increase in acetylene addition than PAH condensation [4] which are considered as two of the major contributors to soot formation. As a consequence, soot production by acetylene addition is the major route at atmospheric pressure followed by PAH condensation and inception. It was further argued that the PAH condensation contribution increases much faster as the pressure is elevated and may exceed the contribution of acetylene addition at high pressures [4] in ethene flames. The acetylene concentrations were shown to be much lower in propene and 1-butene flames as compared to ethene flames at atmospheric conditions, the implication of this fact is currently not

known at higher pressures due to a lack information of acetylene concentrations at elevated pressures in propene and 1-butene flames. Lower acetylene concentrations imply a smaller contribution, through the HACA mechanism, to the high sooting tendencies of propene and 1-butene in comparison to ethene at atmospheric conditions; however, the main culprit could be the relatively larger amounts of aromatics as the pyrolysis products in propene and 1-butene [15,63,64].

Pressure sensitivity of soot yield in ethene flames was found to be slightly higher than those of gaseous alkane (i.e., methane, ethane, and propane) diffusion flames but comparable to that of *n*-heptane flames [37]. However, the pressure sensitivity of soot production in propene and 1-butene diffusion flames are much lower than those of gaseous (i.e., methane, ethane, and propane) and liquid alkane diffusion flames [37]. In view of the reasons discussed above for this unexpected behaviour of C_3 and C_4 olefins, and the compelling evidence that pressure dependence of sooting propensity of aromatics is not as strong as that of alkanes, raise the question whether our current assessment of the effect of aromatic compounds on soot aerosol emissions from diesel and gas turbine engines should be reconsidered. It should be noted that there has been some evidence obtained from diesel engine tests that show very small effects of fuel aromatics on exhaust soot emissions, see e.g., [74,75]. A similar observation, albeit relevant to premixed conditions, was reported by Gao et al. [30]; when a simple aromatic compound, toluene, is blended with *n*-alkanes, the premixed combustion characteristics resemble more to those of *n*-alkanes with reduced influence of the presence of aromatics in the fuel.

The main observations of the current work and the sooting behaviour of single ring aromatics at elevated pressures reported previously and discussed above beg the question whether it is possible that more sooting fuels at atmospheric conditions would have relatively weaker pressure sensitivities as compared to less sooting fuels. More detailed high pressure studies involving highly sooting fuels (and aromatics) at atmospheric conditions would be required to confirm this possiblity.

3.4. Uncertainty in measurements

The maximum uncertainties shown as error bars in Figs. 8 and 19 were evaluated as 3.5% in temperature and about 40% in soot measurements. Using the same experimental setup and data reduction methodologies as the current work, the inferred maximum errors were similar in the previous work originating from this laboratory [39,41–43,46,76]. It should be noted that a significant portion of the evaluated uncertainties results from systematic errors. The main component of the systematic errors in this case is the uncertainty in the soot refractive index, and consequently the refractive index absorption function *E(m)*, which would account for 70–80% of the total uncertainties in soot and temperature measurements. A second component of the systematic errors originates from the overall flame temperature drop with increasing pressure, as discussed in Section 3.1 above. Systematic errors skew the data in one direction, mostly by a scale factor; hence the observed trends in comparisons of the data are not affected by the systematic errors. Therefore, the random error induced uncertainties are relatively small and the comparative trends in measured quantities are statistically sound, and the conclusions based on the observed data trends for sooting tendency dependence of lower olefins on pressure in the current study are reliable. We took the soot refractive index absorption function as 0.27 to have consistency with our previous soot studies conducted at elevated pressures [41,42]. The details of the uncertainty analysis methodologies adopted in this work are available in studies reported previously [41,49].

4. Conclusions

The work reported here is an experimental study conducted for the purpose of assessing the pressure dependence of soot in laminar coflow diffusion flames of lower carbon number olefins, namely ethene, propene, and 1-butene. Since the C_2 – C_4 olefins are among the abundant products of higher alkane pyrolysis their sooting behaviour with pressure is an important aspect in high pressure combustion of hydrocarbon fuels. The pressure range was from atmospheric to 8 bar with ethene and propene flames, and atmospheric to 2.5 bar with 1-butene flames. Temperature and soot volume fraction fields were measured using spectral soot emission technique in flames stabilized in a high-pressure combustion chamber that was used previously for similar experiments.

The main finding of the current experimental work is the results showing the relatively weaker dependence of soot production on pressure in propene and 1-butene flames as compared to ethene flames. This unprecedented behaviour was argued to be an artefact of the formation of significant amounts of single ring aromatics and PAH as the pyrolysis products of propene and 1-butene. Previous studies indicate that the sooting propensities of single ring aromatics show a very weak dependence on pressure in contrast to alkanes.

Comparing the propene and 1-butene results to previous experiments with methane, ethane, and propane flames, the sooting dependence of propene and 1-butene flames on pressure is much weaker than that of gaseous alkanes as well as *n*-heptane. For ethene flames, between 1 and 3 bars the maximum soot yield scales as $\approx P^{2.5}$ and as the pressure is increased, dependence gets weaker; between 4 and 8 bar it is $\approx P^{1.3}$. For propene and 1-butene, on the other hand, scaling is $\approx P^{1}$ from 1 to 2 bar, and with increasing pressure scaling approaches to $P^{0.4}$.

In studies assessing the particulate matter emissions from diesel and gas turbine engines running on conventional middle-distillate hydrocarbon fuels, most of the blame for particulates in the exhaust has been assigned to the aromatic content (and the olefinic content to a certain extent) of the liquid fuels. Reported results of the current study highlights the role played by lower olefins in soot formation in combustion especially at elevated pressures. Although the results and the ensuing arguments are mostly qualitative, the relatively weak dependence of sooting in diffusion flames of C_3 and C_4 olefins and aromatics on pressure would have important implications on evaluating the particulate matter emissions from gas turbines and internal combustion engines fuelled by hydrocarbon-based liquid fuels.

It should be emphasized that computations using detailed chemistry suitable for high pressures should be pursued as a future work for a better understanding of the observed fuel-specific pressure sensitivity of soot formation.

Acknowledgments

The authors thank the Natural Sciences and Engineering Research Council of Canada for a discovery grant (RGPIN-2017-06063) and the Ontario Research Fund for a Research Excellence Program grant (ORF RE07-034), awarded to the senior author, for the support of this research work.

References

[1] A.E. Karataş, Ö.L. Gülder, Soot formation in high pressure laminar diffusion flames, Prog. Energy Combust. Sci. 38 (2012) 818–845.
[2] L.L. McCrain, W.L. Roberts, Measurements of the soot volume field in laminar diffusion flames at elevated pressures, Combust. Flame 140 (2005) 60–69.
[3] R.K.A. Kailasanathan, T. Yelverton, T. Fang, W. Roberts, Effect of diluents on soot precursor formation and temperature in ethylene laminar diffusion flames, Combust. Flame 160 (2013) 656–670.

[4] H. Guo, Z. Gu, K.A. Thomson, G.J. Smallwood, F.F. Baksh, Soot formation in a laminar ethylene/air diffusion flame at pressures from 1 to 8 atm, Proc. Combust. Inst. 34 (2013) 1795–1802.

[5] L. Zhou, N.J. Dam, M.D. Boot, L.P.H. de Goey, Measurements of sooting tendency in laminar diffusion flames of n-heptane at elevated pressure, Combust. Flame 160 (2013) 2507–2516.

[6] L. Zhou, N.J. Dam, M.D. Boot, L.P.H. de Goey, Investigation of the effect of molecular structure on sooting tendency in laminar diffusion flames at elevated pressure, Combust. Flame 161 (2014) 2669–2677.

[7] A.G. Mouis, T.A. Litzinger, Y. Wang, V. Iyer, S. Iyer, M. Linevsky, R.J. Santoro, V. Katta, Effects of a JP-8 surrogate and its components on soot in laminar, N_2-diluted ethylene co-flow diffusion flames from 1 to 5 atm, Combust. Flame 162 (2015) 1987–1995.

[8] F.O. Rice, Thermal decomposition of organic compounds from the standpoint of free radicals. I. Saturated hydrocarbons, J. Am. Chem. Soc. 53 (5) (1931) 1959–1972.

[9] I. Safarik, O.P. Strausz, The thermal decomposition of hydrocarbons. Part 1. *n*-alkanes ($C \geq 5$), Res. Chem. Intermed. 22 (3) (1996) 275–314.

[10] K. Dahm, P. Virk, R. Bounaceur, F. Battin-Leclerc, P. Marquaire, R. Fournet, E. Daniau, M. Bouchez, Experimental and modelling investigation of the thermal decomposition of *n*-dodecane, J. Anal. Appl. Pyrol. 71 (2004) 865–881.

[11] E.C. Fortner, W.A. Brooks, T.B. Onasch, M.R. Canagaratna, P. Massoli, J.T. Jayne, J.P. Franklin, W.B. Knighton, J. Wormhoudt, D.R. Worsnop, C.E. Kolb, S.C. Herndon, Particulate emissions measured during the TCEQ comprehensive flare emission study, Ind. Eng. Chem. Res. 51 (2012) 12586–12592.

[12] S. Yoon, S. Lee, S. Chung, Effect of mixing methane, ethane, propane, and propene on the synergistic effect of PAH and soot formation in ethylene-base counterflow diffusion flames, Proc. Combust. Inst. 30 (2005) 403–410.

[13] S. Kikui, H. Nakamura, T. Tezuka, S. Hasegawa, K. Maruta, Study on combustion and ignition characteristics of ethylene, propylene, 1-butene and 1-pentene in a micro flow reactor with a controlled temperature profile, Combust. Flame 163 (2016) 209–219.

[14] B. Lin, H. Gu, H. Ni, B. Guan, Z. Li, D. Han, C. Gu, C. Shao, Z. Huang, H. Lin, Effect of mixing methane, ethane, propane and ethylene on the soot particle size distribution in a premixed propene flame, Combust. Flame 193 (2018) 54–60.

[15] Y. Wang, S. Park, S.M. Sarathy, S.H. Chung, A comparative study on the sooting tendencies of various 1-alkene fuels in counterflow diffusion flames, Combust. Flame 192 (2018) 71–85.

[16] R.L. Schalla, T.P. Clark, G.E. McDonald, Formation and combustion of smoke in laminar flames, Technical Report 1186, NACA, 1954.

[17] R.L. Schalla, G.E. McDonald, Mechanism of smoke formation in diffusion flames, Symp. (Int.) Combust. 5 (1955) 316–324.

[18] Ö.L. Gülder, Influence of hydrocarbon fuel structural constitution and flame temperature on soot formation in laminar diffusion flames, Combust. Flame 78 (1989) 179–194.

[19] P.C. StJohn, P. Kairys, D.D. Das, C.S. McEnally, L.D. Pfefferle, D.J. Robichaud, M.R. Nimlos, B.T. Zigler, R.L. McCormick, T.D. Foust, Y.J. Bomble, S. Kim, A quantitative model for the prediction of sooting tendency from molecular structure, Energy Fuels 31 (2017) 9983–9990.

[20] L. Ruwe, K. Moshammer, N. Hansen, K. Kohse-Höinghaus, Influences of the molecular fuel structure on combustion reactions towards soot precursors in selected alkane and alkene flames, Phys. Chem. Chem.Phys. 20 (2018) 10780–10795.

[21] E. Bartekova, M. Bajus, Pyrolysis of hexadecane, Collect. Czech. Chem. Commun. 62 (1997) 1057–1069.

[22] K. Hunter, A. East, Properties of C-C bonds in *n*-alkanes: relevance to cracking mechanisms, J. Phys. Chem. A 106 (7) (2002) 1346–1356, doi:10.1021/jp0129030.

[23] J.N. Bradley, Flame and combustion phenomena, Chapman and Hall, London, UK, 1972, Ch. 6.

[24] G. Minkoff, C.F.H. Tipper, Chemistry of combustion reactions, Butterworths, London, UK, 1962, Ch. 9.

[25] S. Zeppieri, High Temperature Experimental and Computational Studies of the Pyrolysis and Oxidation of Endothermic Fuels, Princeton University, 1999 Ph.D. thesis.

[26] I. Glassman, R.A. Yetter, Combustion, 4th edition, Academic Press, New York, 2008, Ch. 7.

[27] X. You, F.N. Egolfopoulos, H. Wang, Detailed and simplified kinetic models of *n*-dodecane oxidation: the role of fuel cracking in aliphatic hydrocarbon combustion, Proc. Combust. Inst. 32 (2009) 403–410.

[28] Y. Yoshihara, K. Nishiwaki, A. Kisei, Modeling of a cracking and auto-ignition process in diesel combustion, 4th International Symposium COMODIA (1998), pp. 123–128.

[29] Y. Yoshihara, M. Ikegami, S. Natake, Kinetics of soot cluster formation at high temperatures, JSME Int. J. Ser. B 37 (2) (1994) 413–419.

[30] Y. Gao, R. Shan, S. Lyra, C. Li, H. Wang, J.H. Chen, T. Lu, On lumped-reduced reaction model for combustion of liquid fuels, Combust. Flame 163 (2016) 437–446.

[31] S. Banerjee, R. Tangko, D.A. Sheen, H. Wang, C.T. Bowman, An experimental and kinetic modeling study of *n*-dodecane pyrolysis and oxidation, Combust. Flame 163 (2016) 12–30.

[32] R. Xu, D. Chen, K. Wang, H. Wang, A comparative study of combustion chemistry of conventional and alternative jet fuels with hybrid chemistry approach, 55th AIAA Aerospace Sciences Meeting on SciTech Forum, AIAA (2017a). 2017-0607

[33] R. Xu, D. Chen, K. Wang, Y. Tao, J.K. Shao, T. Parise, Y. Zhu, S. Wang, R. Zhao, D.J. Lee, F.N. Egolfopoulos, D.F. Davidson, R.K. Hanson, C.T. Bowman, H. Wang, HyChem model: application to petroleum-derived jet fuels, 10th U.S. National Combustion Meeting, Eastern States Section of the Combustion Institute (2017b).

[34] Ö.L. Gülder, K.A. Thomson, D.R. Snelling, Effect of fuel nozzle material properties on soot formation and temperature field in coflow laminar diffusion flames, Combust. Flame 144 (2006) 426–433.

[35] Ö.L. Gülder, Soot formation in laminar diffusion flames at elevated temperatures, Combust. Flame 88 (1992) 75–82.

[36] C.S. McEnally, L.D. Pfefferle, Soot formation in methane/air nonpremixed flames doped with small quantities of C3 hydrocarbons, Combust. Flame 122 (1998) 545–558.

[37] A.E. Karataş, Ö.L. Gülder, Dependence of sooting characteristics and temperature field of co-flow laminar pure and nitrogen-diluted ethylene-air diffusion flames on pressure, Combust. Flame 162 (2015) 1566–1574.

[38] M.R.J. Charest, H. Joo, C.P.T. Groth, Ö.L. Gülder, A numerical study on the effects of pressure and gravity in laminar ethylene diffusion flames, Proc. Combust. Inst. 33 (2011) 549–557.

[39] H. Joo, Ö.L. Gülder, Experimental study of soot and temperature field structure of laminar co-flow ethylene–air diffusion flames with nitrogen dilution at elevated pressures, Combust. Flame 158 (2011) 416–422.

[40] C. Kim, F. Xu, G. Faeth, Soot surface growth and oxidation at pressures up to 8.0 atm in laminar nonpremixed and partially premixed flames, Combust. Flame 152 (2008) 301–316.

[41] K.A. Thomson, Ö.L. Gülder, R.A. Weckman, E.J. Fraser, G.J. Smallwood, D.R. Snelling, Soot concentration and temperature measurements in co-annular, nonpremixed CH_4/air laminar diffusion flames at pressures up to 4 MPa, Combust. Flame 140 (2005) 222–232.

[42] P.M. Mandatori, Ö.L. Gülder, Soot formation in laminar ethane diffusion flames at pressures from 0.2 to 3.3 MPa, Proce. Combust. Inst. 33 (2011) 577–584.

[43] A.E. Karatas, G. Intasopa, Ö.L. Gülder, Sooting behaviour of *n*-heptane laminar diffusion flames at high pressures, Combust. Flame 160 (2013) 1650–1656.

[44] F. Liu, A.E. Karataş, Ö.L. Gülder, M. Gu, Numerical and experimental study of the influence of CO_2 and N_2 dilution on soot formation in laminar coflow C_2H_4/air diffusion flames at pressures between 5 and 20 atm, Combust. Flame 162 (2015) 2231–2247.

[45] P.H. Joo, M.R.J. Charest, C.P.T. Groth, Ö.L. Gülder, Comparison of structures of laminar methane-oxygen and methane-air diffusion flames from atmospheric to 60 atm, Combust. Flame 160 (2013) 1990–1998.

[46] H.I. Joo, Ö.L. Gülder, Soot formation and temperature field structure in co-flow laminar diffusion flames at pressures from 10 to 60 atmospheres, Proc. Combust. Inst. 32 (2009) 769–775.

[47] Ö.L. Gülder, G. Intasopa, H.I. Joo, P.M. Mandatori, D.S. Bento, M.E. Vaillancourt, Unified behaviour of maximum soot yields of methane, ethane, and propane laminar diffusion flames at high pressures, Combust. Flame 158 (2011) 2037–2044.

[48] P.H. Joo, Ö.L. Gülder, Formation of liquid methane water mixture during combustion of a laminar methane jet at supercritical pressures, Energy Fuels 26 (2012) 5462–5467.

[49] D. Snelling, K. Thompson, G. Smallwood, Ö.L. Gülder, Spectrally resolved measurement of flame radiation to determine soot temperature and concentration, AAIA J. 40 (9) (2002) 1789–1795.

[50] R.W. Davis, E.F. Moore, R.J. Santoro, J.R. Ness, Isolation of buoyancy effects in jet diffusion flame experiments, Combust. Sci. Technol. 73 (1990) 625–635.

[51] N. Vargaftik, Y. Vinogradov, V. Yargin, Handbook of physical properties of liquids and gases, 3rd augmented and revised, Begell House, 1996.

[52] K. Steele, B.E. Poling, D.B. Manley, Vapor pressures for the system 1-butene, isobutene, and 1,3-butadiene, J. Chem. Eng. Data 21 (4) (1976) 399–403.

[53] P.H. Joo, B. Gigone, E.A. Griffin, M. Christensen, Ö.L. Gülder, Soot primary particle size dependence on combustion pressure in laminar ethylene diffusion flames, Fuel 220 (2018) 464–470, doi:10.1016/j.fuel.2018.02.025.

[54] I. Glassman, Sooting laminar diffusion flames: effect of dilution, additives, pressure and microgravity, Symp. (Int.) Combust. 27 (1998) 1589–1596.

[55] R.J. Santoro, H.G. Semerjian, Soot formation in diffusion flames: Flow rate, fuel species and temperature effects, Symp. (Int.) Combust. 20 (1984) 997–1006.

[56] W.L. Flower, Soot particle temperatures in axisymmetric laminar ethylene-air diffusion flames at pressures up to 0.7 MPa, Combust. Flame 77 (1989) 279–293.

[57] W.L. Flower, C.T. Bowman, Soot production in axisymmetric laminar diffusion flames at pressures from one to ten atmospheres, Proc. Combust. Inst. 21 (1988) 1115–1124.

[58] A.E. Karataş, Ö.L. Gülder, Effects of carbon dioxide and nitrogen addition on soot processes in laminar diffusion flames of ethylene-air at high pressures, Fuel 200 (2017) 76–80.

[59] R. Axelbaum, C. Law, Soot formation and inert addition in diffusion flames, Symp. (Int.) Combust. 23 (1990) 1517–1523.

[60] Ö.L. Gülder, D.R. Snelling, Influence of nitrogen dilution and flame temperature on soot formation in diffusion flames, Combust. Flame 92 (1993) 115–124.

[61] M.R.J. Charest, C.P.T. Groth, Ö.L. Gülder, A numerical study on the effects of pressure and gravity in laminar ethylene diffusion flames, Combust. Flame 158 (2011) 1933–1945.

[62] Ö.L. Gülder, Corrigendum to dependence of sooting characteristics and temperature field of co-flow laminar pure and nitrogen-diluted ethylene-air diffusion flames on pressure, Combust. Flame 173 (2016) 1.

[63] K. Wang, S.M. Villano, A.M. Dean, Fundamentally-based kinetic model for propene pyrolysis, Combust. Flame 162 (2015) 4456–4470.
[64] K. Wang, S.M. Villano, A.M. Dean, Experimental and kinetic modeling study of butene isomer pyrolysis: Part I. 1- and 2-Butene, Combust. Flame 173 (2016) 347–369.
[65] S. Sinha, R.K. Rahman, A. Raj, On the role of resonantly stabilized radicals in polycyclic aromatic hydrocarbon (PAH) formation: pyrene and fluoranthene formation from benzylindenyl addition, Phys. Chem. Chem. Phys. 19 (2017) 19262–19278.
[66] M. Schenk, L. Leon, K. Moshammer, P. Oßwald, T. Zeuch, L. Seidel, F. Mauss, K. Kohse-Höinghaus, Detailed mass spectrometric and modeling study of isomeric butene flames, Combust. Flame 160 (2013) 487–503.
[67] Y. Zhang, J. Cai, L. Zhao, J. Yang, H. Jin, Z. Cheng, Y. Li, L. Zhang, F. Qi, An experimental and kinetic modeling study of three butene isomers pyrolysis at low pressure, Combust. Flame 159 (2012) 905–917.
[68] A.E. Daca, Ö.L. Gülder, Soot formation characteristics of diffusion flames of methane doped with toluene and *n*-heptane at elevated pressures, Proc. Combust. Inst. 36 (2017) 737–744.
[69] M. Frenklach, S. Taki, R.A. Matula, A conceptual model for soot formation in pyrolysis of aromatic hydrocarbons, Combust. Flame 49 (1983) 275–282.
[70] T.S. Wang, Soot formation from toluene, Loussianna State University, 1980 Ph.D. thesis.
[71] T.S. Wang, R.A. Matula, R.C. Farmer, Combustion kinetics of soot formation from toluene, Symp. (Int.) Combust. 18 (1981) 1149–1158.
[72] Y.G. Knorre, D. Tanke, T. Thienel, H.G. Wagner, Soot formation in the pyrolysis of benzene/acetylene and acetylene/hydrogen mixtures at high carbon concentrations, Symp. (Int.) Combust. 26 (1996) 2303–2310.
[73] D. Tanke, Rußbildung in der Kohlenwasserstoffpyrolyse hinter Stoßwellen, Georg-August-Universität zu Göttingen, 1994 Ph.D. thesis.
[74] X. Li, W.L. Chippior, Ö.L. Gülder, J. Cooley, E.K. Richardson, K. Mitchell, Comparison of the exhaust emissions of diesel fuels derived from oil sands and conventional crude oil, International Fall Fuels and Lubricants Meeting and Exposition, SAE International (1998), doi:10.4271/982487.
[75] W.S. Neill, W.L. Chippior, Ö.L. Gülder, J. Cooley, E.K. Richardson, K. Mitchell, C. Fairbridge, Influence of fuel aromatics type on the particulate matter and NO_x emissions of a heavy-duty diesel engine, CEC/SAE Spring Fuels & Lubricants Meeting & Exposition, SAE International (2000), doi:10.4271/2000-01-1856.
[76] D.S. Bento, K.A. Thomson, Ö.L. Gülder, Soot formation and temperature field structure in laminar propane-air diffusion flames at elevated pressures, Combust. Flame 145 (2006) 765–778.